Explainable AI applications for Serial Femtosecond X-ray Crystallography

Harald Agelii [1] **Alfredo Bellisario** [1] **Carl Caleman** [1 2] **Nicusor Timneanu** [1] **Sebastian Cardoch** [1]
[1]*Department of Physics and Astronomy, Uppsala University, Box 516, 75120 Uppsala, Sweden* [2]*Center for Free-Electron Laser Science CFEL, Deutsches-Elektronen Synchrotron DESY, Notkestr. 85, 22607 Hamburg, Germany*. Correspondence to: Alfredo Bellisario alfredo.bellisario@physics.uu.se, Nicusor Timneanu nicusor.timneanu@physics.uu.se, Sebastian Cardoch sebastian.cardoch@physics.uu.se.

1. Introduction

Serial Femtosecond X-ray crystallography (SFX) is an experimental technique that captures the structure of protein crystals at room temperature. This technique uses X-ray Free Electron Lasers (XFELs), powerful light sources that produce ultra-short and high-brilliance X-ray pulses, to capture single diffraction patterns from thousands of weakly diffracting small crystals before they are destroyed-a process known as "diffraction before destruction" [1]. Advances in AI for biophysics, in particular AlphaFold [2], [3] which incorporates data partially derived from X-ray sources, are shifting the focus of scientific research from static structures to exploring protein dynamics at high resolution, a vastly unexplored field for which limited data is available. Although powerful and already routinely used for studying the conformational landscape of proteins, SFX experiments are affected by inherent fluctuations in X-ray pulse generation which requires accurate monitoring of the beam fluence and pulse duration.

X-ray emission spectra (XES) have been used in concurrence with SFX [4], [5] enabling the characterization of the electronic structure of proteins. The high sensitivity of XES to the beam properties provides a way for beam diagnostics. A simple schematic of the experimental set-up is shown on Fig. 1. This study has a two-fold goal. First we explore the feasibility of using XES from protein crystals for real-time shot-to-shot X-ray pulse characterization. To do this, we train a deep neural network on synthetic emission spectra to predict fluence and pulse duration. The second goal delves into the gaining physical insights from the trained model. We apply explainable AI techniques [6] to identify spectral features influencing predictions. Ultimately, this work highlights the potential of extracting critical X-ray pulse parameters, providing a reliable and interpretable AI-driven approach for enhancing XFEL experiments and advancing real-time diagnostics.

2. Methodology

XES can be performed in principle at any region available with an X-ray light source, but the low photon count from X-ray exposure requires the use of high-repetition rates and several of shot averages [5]. We therefore decided to focus our efforts in the sulfur Kα emission region which has already been detected from single shots of ammonium sulfate [7]. Plasma simulations, based on non-local thermodynamic equilibrium collisional radiative code [8], [9],

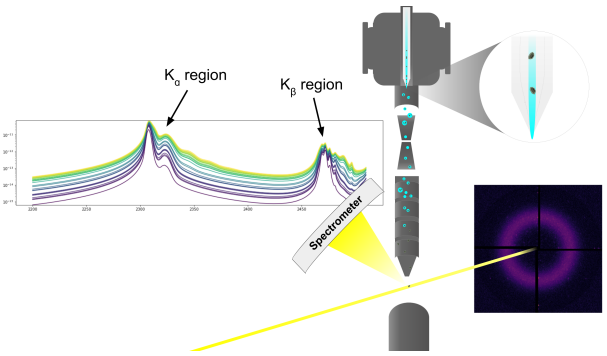

Fig. 1: Combined SFX and XES scheme. A liquid jet injection system delivers microcrystals (shown in the inset at the top right) into the path of the ultrafast X-ray beam. The resulting diffraction pattern is recorded on a 2D detector (bottom right), while emitted X-rays from the sample are directed toward a spectrometer for XES measurements (on the left). The overlaid spectra represent X-ray emission spectra from our own dataset.

were performed to generate two datasets of sulfur K-shell emission spectra from a lysozyme crystal under varying X-ray fluence and pulse duration. This code has been routinely used to provide insight on XFEL experiments [10]–[12] and tested within the sulfur K-shell, providing good match with experiments. The first dataset consists of 6000 time-integrated K shell sulfur emission spectra. For the generation of the synthetic data, we uniformly sample the fluence range $5\,e3 - 5\,e5\ \mathrm{J\,cm^{-2}}$, to obtain an even sampling of the fluence, and fix the pulse duration to $10\,\mathrm{fs}$, photon energy to $12\,\mathrm{keV}$ and bandwidth to $1\,\%$. We also generated a dataset with varying fluence and pulse duration, using $21\,000$ emission spectra sampled from $5\,e2 - 5\,e5\ \mathrm{J\,cm^{-2}}$ fluence and 3–30 fs pulse duration. These spectra serve as input for a fully connected feedforward neural network trained to predict in a first instance only fluence, and then retrained to predict fluence and pulse duration concurrently. Experimental emission spectra often require calibration, which may not always be feasible in real-time. To get closer to an experimental scenario, we pre-process the synthetic spectra by: linearly interpolating to 1000 uniform points, applying min-max normalization to decouple intensity from emission magnitude, augmenting data by introducing random shifts to remove baseline dependence, and adding noise with a 0.1% standard deviation. We construct a fully connected feedforward neural network with four hidden layers

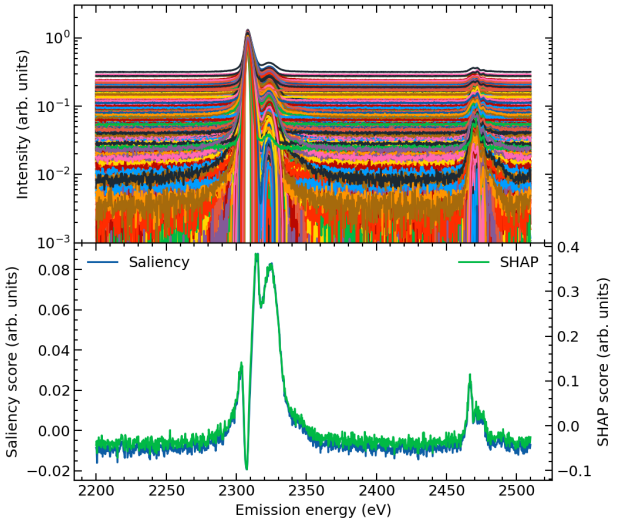

Fig. 2: The top panel displays stacked X-ray emission spectra across a range of emission energies, with sulfur emission intensity shown in arbitrary units. The lower panel plots two model interpretability metrics—gradient-based (blue) and SHAP (green)—indicating the regions of interest in the spectra that most strongly influence the model's predictions.

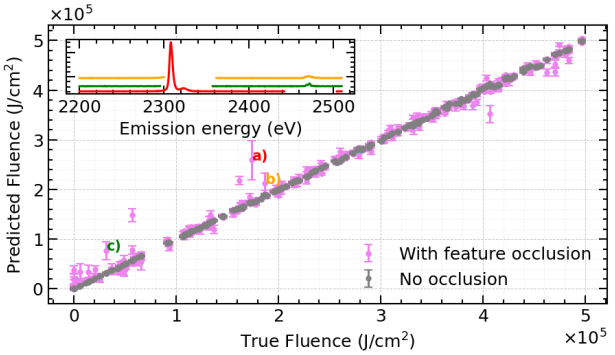

Fig. 3: Ensemble predictions with and without applying feature occlusion to the spectra were compared to fluence levels. The dots correspond to the ensemble's mean and the error bars to the standard deviation of each prediction. At lower fluence, the relative uncertainty increases, yet the uncertainty is higher when the Kα or Kβ regions are completely occluded, as illustrated in the inset. The inset displays three examples for each labeled prediction in the plot with corresponding color-coded letters.

containing 384, 128, 1024 and 448 nodes. The choice of the number of layers and nodes was motivated by hyperparameter tuning performed using *KerasTuner* [13]. The hidden layers employ ReLU activations, and the output layer uses a linear activation. The dataset is split into 80% training and 20% testing. A 10-fold cross-validation ensures robustness. Training is performed with mean squared error loss, batch size 16, and 500 epochs, optimized using Adam with a dynamic learning rate ranging from 10^{-3} to 10^{-5}, decreasing when validation loss stagnates. We gain interpretation of our model using gradient-based, SHAP, and feature occlusion methods.

3. Results and Discussion

3.1 Predicting X-ray Pulse Fluence and Pulse Duration

Our model provides fluence estimates with a standard deviation of $1.41\,\%$, for comparison, current experimental methods for diagnostics and monitoring of beamlines [14]–[17] assume no transmission losses through the X-ray optics and provide an absolute accuracy of only slightly less than $10\,\%$ [14]. For concurrent predictions, the model achieves relative errors of $11.8\,\%$ for fluence and $9.4\,\%$ for pulse duration. We analyze feature importance using Gradient and SHAP interpretation methods, as shown in Fig. 2. The model assigns highest importance to Kα transitions, particularly shifts at 2.29–$2.35\,\mathrm{keV}$ caused by highly charged sulfur ions. These results confirm fluence-dependent spectral broadening and indicate the potential for using sulfur XES as a diagnostic tool. SHAP analysis reveals distinct spectral signatures for fluence and pulse duration predictions. While fluence correlates with K to L shifts, pulse duration is linked to $K^2L_{2,3}$ double core hole emissions. Shorter pulses lead to increased core-hole creation before relaxation, altering emission signatures. These findings demonstrate that neural networks can extract pulse characteristics directly from sulfur XES, offering a pathway for real-time XFEL diagnostics.

3.2 Feature occlusion

To investigate the model's robustness and its dependence on specific spectral regions, we occluded random parts in the input spectra. We doubled the original dataset creating a copy of each spectrum and randomly masking 20% by setting these values to zero. We then applied 10 fold cross-validation on the dataset with partially occluded spectra. Fig. 3 shows the ensemble-averaged predictions along with their standard deviations for the test dataset. Most of the ensemble predictions show small uncertainty, although few outliers are present. Closer inspection of these outliers (in the figure inset) indicates that they occur when $K^2L_{2,3}$ double core hole emissions or double core hole L to K (K^2ML_l) and single core hole M to K (KM_l) emission lines are completely removed. This observation is consistent with our earlier insights from SHAP and saliency, reaffirming the model remains largely robust if at least part of the Kα and Kβ regions are present.

Acknowledgments

The authors thank Howard A. Scott, Jan-Erik Rubensson, Tomas André, and the Uppsala University Biophysics Network for discussions. This work was funded by the Swedish Research Council (Grants 2019-03935, 2023-03900, 2018-00740), the Röntgen-Ångström Cluster (Grant 2019-03935), and

the Helmholtz Association. Computing resources were provided by the Davinci cluster at Uppsala University.

References

[1] R. Neutze, R. Wouts, D. van der Spoel, *et al.*, "Potential for biomolecular imaging with femtosecond X-ray pulses," *Nature*, vol. 406, no. 6797, pp. 752–757, Aug. 2000, ISSN: 1476-4687. DOI: 10.1038/35021099. [Online]. Available: https://doi.org/10.1038/35021099.

[2] J. Jumper, R. Evans, A. Pritzel, *et al.*, "Highly accurate protein structure prediction with alphafold," *nature*, vol. 596, no. 7873, pp. 583–589, 2021.

[3] J. Abramson, J. Adler, J. Dunger, *et al.*, "Accurate structure prediction of biomolecular interactions with alphafold 3," *Nature*, vol. 630, no. 8016, pp. 493–500, 2024.

[4] J. Kern, R. Alonso-Mori, R. Tran, *et al.*, "Simultaneous Femtosecond X-ray Spectroscopy and Diffraction of Photosystem II at Room Temperature," *Science*, vol. 340, no. 6131, pp. 491–495, Apr. 2013. DOI: 10.1126/science.1234273. [Online]. Available: https://doi.org/10.1126/science.1234273 (visited on 09/13/2023).

[5] T. Fransson, R. Chatterjee, F. D. Fuller, *et al.*, "X-ray Emission Spectroscopy as an in Situ Diagnostic Tool for X-ray Crystallography of Metalloproteins Using an X-ray Free-Electron Laser," *Biochemistry*, vol. 57, no. 31, pp. 4629–4637, Aug. 2018, ISSN: 0006-2960. DOI: 10.1021/acs.biochem.8b00325. [Online]. Available: https://doi.org/10.1021/acs.biochem.8b00325.

[6] W. Samek, G. Montavon, S. Lapuschkin, *et al.*, "Explaining Deep Neural Networks and Beyond: A Review of Methods and Applications," *Proceedings of the IEEE*, vol. 109, no. 3, pp. 247–278, Mar. 2021, ISSN: 1558-2256. DOI: 10.1109/JPROC.2021.3060483.

[7] B. Abraham, S. Nowak, C. Weninger, *et al.*, "A high-throughput energy-dispersive tender X-ray spectrometer for shot-to-shot sulfur measurements," *Journal of Synchrotron Radiation*, vol. 26, no. 3, pp. 629–634, May 2019. DOI: 10.1107/S1600577519002431. [Online]. Available: https://doi.org/10.1107/S1600577519002431.

[8] H. A. Scott and R. W. Mayle, "GLF - A simulation code for X-ray lasers," *Applied Physics B*, vol. 58, no. 1, pp. 35–43, Jan. 1994, ISSN: 1432-0649. DOI: 10.1007/BF01081711. [Online]. Available: https://doi.org/10.1007/BF01081711.

[9] H. A. Scott, "Cretin—a radiative transfer capability for laboratory plasmas," *Radiative Properties of Hot Dense Matter*, vol. 71, no. 2, pp. 689–701, Oct. 2001, ISSN: 0022-4073. DOI: 10.1016/S0022-4073(01)00109-1. [Online]. Available: https://www.sciencedirect.com/science/article/pii/S0022407301001091.

[10] A. Barty, C. Caleman, A. Aquila, *et al.*, "Self-terminating diffraction gates femtosecond X-ray nanocrystallography measurements," *Nature Photonics*, vol. 6, no. 1, pp. 35–40, Jan. 2012, ISSN: 1749-4893. DOI: 10.1038/nphoton.2011.297. [Online]. Available: https://doi.org/10.1038/nphoton.2011.297.

[11] K. R. Beyerlein, H. O. Jönsson, R. Alonso-Mori, *et al.*, "Ultrafast nonthermal heating of water initiated by an X-ray Free-Electron Laser," *Proceedings of the National Academy of Sciences*, vol. 115, no. 22, pp. 5652–5657, May 2018. DOI: 10.1073/pnas.1711220115. [Online]. Available: https://doi.org/10.1073/pnas.1711220115 (visited on 02/26/2025).

[12] I. Dawod, S. Cardoch, T. André, *et al.*, "MolDStruct: Modeling the dynamics and structure of matter exposed to ultrafast x-ray lasers with hybrid collisional-radiative/molecular dynamics," *The Journal of Chemical Physics*, vol. 160, no. 18, p. 184 112, May 2024, ISSN: 0021-9606. DOI: 10.1063/5.0197225. [Online]. Available: https://doi.org/10.1063/5.0197225 (visited on 02/26/2025).

[13] T. O'Malley, E. Bursztein, J. Long, *et al.*, *Keras tuner*, https://github.com/keras-team/keras-tuner, 2019.

[14] J. Grünert, M. P. Carbonell, F. Dietrich, *et al.*, "X-ray photon diagnostics at the European XFEL," *Journal of Synchrotron Radiation*, vol. 26, no. 5, pp. 1422–1431, Sep. 2019. DOI: 10.1107/S1600577519006611. [Online]. Available: https://doi.org/10.1107/S1600577519006611.

[15] T. Maltezopoulos, F. Dietrich, W. Freund, *et al.*, "Operation of X-ray gas monitors at the European XFEL," *Journal of Synchrotron Radiation*, vol. 26, no. 4, pp. 1045–1051, Jul. 2019. DOI: 10.1107/S1600577519003795. [Online]. Available: https://doi.org/10.1107/S1600577519003795.

[16] J. Grünert, W. Freund, J. Liu, *et al.*, "Absolute photon power measurements at the European XFEL instruments," *Journal of Physics: Conference Series*, vol. 2380, no. 1, p. 012 083, Dec. 2022, ISSN: 1742-6596. DOI: 10.1088/1742-6596/2380/1/012083. [Online]. Available: https://dx.doi.org/10.1088/1742-6596/2380/1/012083.

[17] Yiping Feng, Jan M Feldkamp, David M. Fritz, *et al.*, "A single-shot intensity-position monitor for hard x-ray FEL sources," vol. 8140, Oct. 2011, 81400Q. DOI: 10.1117/12.893740. [Online]. Available: https://doi.org/10.1117/12.893740.